Nano Energy 40 (2017) 327–335

Contents lists available at ScienceDirect

Nano Energy

journal homepage: www.elsevier.com/locate/nanoen

Full paper

Functionalized fullerenes for highly efficient lithium ion storage: Structure-property-performance correlation with energy implications

Changsheng Shan[a], Hung-Ju Yen[a], Kaifeng Wu[b], Qianglu Lin[a], Ming Zhou[c], Xiaofeng Guo[d], Di Wu[e], Hanguang Zhang[f], Gang Wu[f,*], Hsing-Lin Wang[a,g,*]

[a] Physical Chemistry and Applied Spectroscopy, Chemistry Division, Los Alamos National Laboratory, Los Alamos, NM 87545, United States
[b] State Key Laboratory of Molecular Reaction Dynamics, Dalian Institute of Chemical Physics, Chinese Academy of Sciences, Dalian 116023, China
[c] Department of Chemistry, Northeast Normal University, Changchun, Jilin 130024, China
[d] Earth and Environmental Sciences Division, Los Alamos National Laboratory, Los Alamos, NM 87545, United States
[e] The Gene and Linda Voiland School of Chemical Engineering and Bioengineering, Washington State University, Pullman, WA 99163, United States
[f] Department of Chemical and Biological Engineering, University at Buffalo, The State University of New York, Buffalo, NY 14260, United States
[g] Department of Materials Science and Engineering, Southern University of Science and Technology, Shenzhen, Guangdong 518055, China

ARTICLE INFO

Keywords:
Fullerene
Functionalization
Anode material
Lithium ion battery
Energy storage

ABSTRACT

Here, we report that spherical C_{60} derivatives with well-defined molecular structures hold great promise to be advanced anode materials for lithium-ion batteries (LIBs). We studied four C_{60} molecules with various functional groups, including pristine, carboxyl, ester, and piperazine C_{60}. The comparison of these C_{60}s elucidated a strong correlation between functional group, overall packing (crystallinity), and the anode performance in LIBs. Specifically, carboxyl C_{60} and neutral ester C_{60} showed higher charge capacities than pristine C_{60}, whereas positively-charged piperazine C_{60} exhibited lower capacity. The highest charge capacity was achieved on the carboxyl C_{60} (861 mAh g^{-1} at 100th cycle), which is five times higher than that of pristine C_{60} (170 mAh g^{-1}), more than double the theoretical capacity of commercial graphite (372 mAh g^{-1}), and even higher than the theoretical capacity of graphene (744 mAh g^{-1}). Carboxyl C_{60} also showed a high capacity at a fast discharge-charge rate (370 mAh g^{-1} at 5 C). The exceptional performance of carboxyl C_{60} can be attributed to multiple key factors. They include the complex formation between lithium ions and oxygen atoms on the carboxyl group, the improved lithium-binding capability of C_{60} cage due to electron donating from carboxylate groups, the electrostatic attraction between carboxylate groups and lithium ions, and the large lattice void space and high specific area due to carboxyl functionalization. This study indicates that, while maintaining the basic C_{60} electronic and geometric properties, functionalization with desired groups can achieve remarkably enhanced capacity and rate performance for lithium storage.

1. Introduction

Lithium ion batteries (LIBs) have been considered as key candidates for energy storage and power supply for applications in portable electronic devices and electric vehicles [1–6]. In particular, the ever-increasing demand in electric vehicles has greatly promoted the research interests for developing advanced LIBs with high reversible capacity, excellent rate capability, and cycling stability [7–12]. Carbon-based anode materials have raised a great deal of interests due to their low-cost and light-weight (i.e. high energy density). However, graphite, the most commonly studied anode materials for LIBs has some drawbacks such as low theoretical specific capacity (372 mAh g^{-1}), lack of long term stability, and poor rate performance [13–16]. To this aim, many efforts have been devoted to developing anode materials, such as carbon allotropy, silicon, metal oxides, and organic compounds [17–28].

Among various anode materials, carbon-based LIBs have gained extensive attention because metallic lithium is replaced by a carbon host structure that can reversibly absorb and release lithium ions at low electrochemical potentials [29–31]. In addition, in contrast to their inorganic counterparts, carbon based materials have the advantages of low-cost, lightweight, and the ability to be functionalized with tunable electrical, electronic and redox properties. Improved cycling stability and capacity have been achieved by using nanoporous and heteroatom-doped carbon materials with various microstructures, such as graphene [32–34], graphene nanoribbons [35], carbon nanotubes [36,37],

* Corresponding authors.
E-mail addresses: gangwu@buffalo.edu (G. Wu), wangxl3@sustc.edu.cn (H.-L. Wang).

http://dx.doi.org/10.1016/j.nanoen.2017.08.033
Received 25 June 2017; Received in revised form 10 August 2017; Accepted 18 August 2017
Available online 19 August 2017

nanofibers [7,38], nanobeads [39], hollow nanospheres [40], porous carbon [41–43], carbon nanoparticles [44], porous carbon cloth [45], and their hybrids [46,47]. Despite all the advancements in optimizing the above carbon-based materials, their structural heterogeneity remains a challenge for lack of control over their structures at the molecular level. Thus, the underlying mechanisms responsible for those improvements have not been well established, which hinders a greater understanding between the structure and LIB properties of materials [48–50]. For example, reduced graphene oxides have ill-defined molecular structures with a lot of defects; therefore, it is not possible to establish structure–property relationships and raises a great concern over their performance reproducibility.

Notably, most of previously studied carbon materials for LIBs are layered structures, such as graphite and graphene, presumably allow for facile diffusion and incorporation of lithium ions. Unlike many layer-structured carbon materials, C_{60} has a precisely-defined zero-dimensional spherical structure. The C_{60} molecule is composed of a carbon cage with 20 hexagons and 12 pentagons on its surface [51,52]. The pure C_{60} and its derivatives can be synthesized with precisions down to the molecular level, and hence alleviate the aforementioned structural heterogeneity issue associated with many carbon materials. Since their discovery, C_{60}-based fullerenes have been extensively studied primarily for biomedical applications [53,54] and for the electron transport layers in photovoltaic devices [55–57]. Chabre et al., first reported that C_{60} may be used for LIBs as they showed electrochemical intercalation of lithium into solid C_{60}, suggesting that each C_{60} molecule can bind with 12 lithium to form $C_{60}Li_{12}$ corresponding to a capacity of 446 mAh/g [58]. In addition, the capacity of C_{60} molecule can be increased by hydrogenation of C_{60} at 1200 mAh/g [59]. However, it is very important to note that hydrogenated C_{60} does not have any electronic and/or optical properties of C_{60}. It is simply a hydrocarbon with a caged structure. Lacking of experimental details and structural data of hydrogenated C_{60} from this report, it is simply not possible to draw meaningful conclusions on how C_{60} can be modified to render a much improved energy storage materials.

In recent years, C_{60} has been used as the additive to boost the charge capacity of reduced graphene oxide/graphite in LIBs because C_{60} can function as a spacer to increase inter-layer distances between graphene layers and to facilitate the incorporation of lithium ions [48]. In addition, C_{60} based polymers were mixed with silicon powders to increase the stability of silicon based LIBs [60]. However, there is no systematic study about the relationship between the functional groups and device performance in carbon-based LIBs. The structure-property correlation would be extremely helpful to provide insights for optimizing and exploring new materials for next generation LIBs.

In this work, we report for the first time a systematic study on spherical C_{60} and its derivatives with well-defined molecular structures as anode materials for LIBs. Four different C_{60} derivatives including pristine C_{60}, ester C_{60}, carboxyl C_{60}, and positively-charged piperazine C_{60} were used as anode materials to study their performances in LIBs (Fig. 1a). The structures of these C_{60} and C_{60} derivatives were synthesized and characterized. Their molecular and hierarchical structures have been confirmed by nuclear magnetic resonance spectroscopy (NMR), transmission electron microscopy (TEM), UV–visible spectroscopy, and X-ray diffraction (XRD). The carboxyl C_{60} and ester C_{60} showed much higher lithium storage capacity than pristine C_{60} presumably due to the O=C-O functional groups, which not only provide the binding sites for lithium ions, but also change the electronic and crystalline structures, surface charge, and specific surface area of C_{60} to improve the capacity of C_{60} derivatives. In contrast, the highly-crystalline pristine C_{60} and positively-charged piperazine C_{60} have an adverse effect on the capacity. These strong correlations between functionalized groups in C_{60} and LIB performances suggest that C_{60} with desired functionality at the molecular level can achieve significantly enhanced lithium-ion storage capacity.

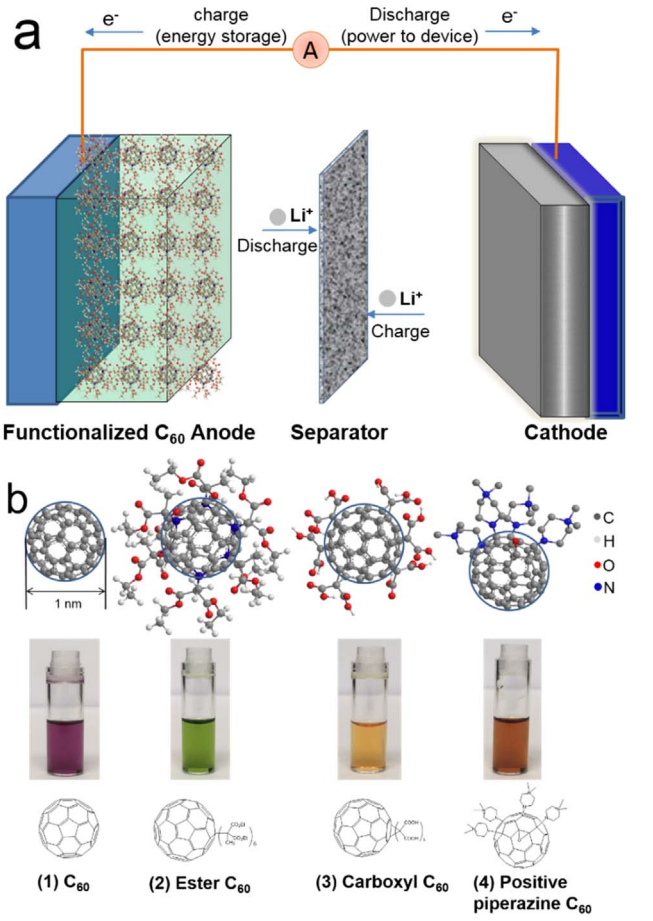

Fig. 1. (a) A schematic representation of C_{60}-based LIBs; (b) ball-and-stick models (top), pictures of dispersed solutions (middle), and molecular structures (bottom) of C_{60} (1), ester C_{60} (2), carboxyl C_{60} (3), and positive piperazine C_{60} (4). 1, 2, and 4 are in 1, 2-dichlorobenzene; 3 is in water.

2. Material and methods

2.1. Chemicals and materials

Fullerene C_{60} (99%) was purchased from BuckyUSA company. Polyvinylidene fluoride (PVDF, fluoride content, 59%) was purchased from Scientific Polymer Products, Inc. Tetrabutylammonium perchlorate ($TBAClO_4$), electrolyte (1 M $LiPF_6$ in 1:1 (v/v) mixture of ethylene carbonate/dimethyl carbonate (EC/DMC) solution) for coin cell battery test, and other solvents were all purchased from Sigma–Aldrich and used as received if not specified. The materials for battery test including carbon coated copper foil, conductive acetylene black, and coin cell cases were purchased from MTI corporation.

2.2. Characterization

^{13}C NMR spectra were measured on a Bruker AC-400 MHz spectrometer in the indicated solvent, using tetramethylsilane as an internal reference. UV–vis–NIR measurements for C_{60} and C_{60} derivatives in tetrahydrofuran (THF) solution were collected with a Varian Cary 5000 spectrometer. X-ray diffraction (XRD) patterns of the samples were conducted on a Rigaku Ultima III X-ray diffractometer using fine-line-sealed Cu Kα tube (λ = 1.54178 Å) X-rays. The transmission electron microscopy (TEM) was examined by using a JOEL JEM-1230 transmission electron microscope. The Brunauer-Emmett-Teller (BET) surface area of each sample was measured at −196 °C by using a Micromeritics ASAP 2020 instrument and samples were degassed at 100 °C to remove any adsorbates prior to any experiments. Cyclic

voltammetry measurements were performed using a N_2-filled three-electrode cell with a platinum wire as the auxiliary electrode and an Ag/AgCl wire as reference in a CHI 760e electrochemical workstation. The solvent, acetonitrile was distilled before use. The concentrations of pristine C_{60} and C_{60} derivatives were 0.3 mg/mL. Working electrode was glassy carbon electrodes (d = 3 mm). Before use, glassy carbon electrode was carefully polished to a mirror finish with 1.0, 0.3, and 0.05 μm alumina slurries, successively.

2.3. Synthesis of C_{60} derivatives

$C_{60}[C(CH_3)(CO_2\text{-}t\text{-}Bu)_2]_6$ (ester C_{60}) [61], ($C_{60}[C(CO_2H)_2]_6$) (carboxyl C_{60}) [62], and C_{60}(*N*-methylpiperazine)$_4$ [63] were synthesized according to the previously reported procedure.

2.3.1. $C_{60}[C(CH_3)(CO_2\text{-}t\text{-}Bu)_2]_6$ (ester C_{60})

Synthesis of ester C_{60} was made by the treatment of deoxygenated C_{60} solution in toluene-THF with sodium naphthalenide (10 equiv) for 2 h at ambient temperature. To the blackish suspension was added excess amount of di-*tert*-butyl 2-bromo-2-methylmalonate, and it was allowed to react for an additional 12 h at ambient temperature. After workup and separation of the solids by precipitation cycles, the products were then purified by repetitive chromatography to afford ester C_{60} with roughly 30% in yield. ^{13}C NMR (100 MHz, $CDCl_3$): δ 168.84, 156.35, 152.37, 146.38, 142.76, 131.01, 82.24, 61.44, 57.14, 28.07, 20.38.

2.3.2. $C_{60}[C(CO_2H)_2]_6$ (carboxyl C_{60})

Synthesis of $C_{60}[C(CO_2Et)_2]_6$ was made by the treatment of C_{60} solution in toluene with 9,10-dimethylanthracene (10 equiv) for 2.0 h at ambient temperature. To the blackish suspension was added CBr_4 and diethyl malonate (10 equiv) with excess amount of 1,8-diazabicyclo-[5.4.0]undec-7-ene, and the reaction was allowed to react for an additional 12 h at ambient temperature. After workup and separation of the solids by precipitation cycles, the products were purified by repetitive chromatography using toluene-ethyl acetate as eluent to afford $C_{60}[C(CO_2Et)_2]_6$ in a yield of 43%.

Carboxyl C_{60} was then prepared by the hydrolysis of $C_{60}[C(CO_2Et)_2]_6$ with excess amount of sodium hydride in a nitrogen atmosphere in dry toluene. The reaction mixture was quenched by methanol in air after heated with stirring at 60 °C for 3 h. After centrifugation and concentration, the precipitate was sequentially washed with toluene, 2 M H_2SO_4, water, and finally dried under vacuum at 60 °C for 12 h to afford the desired product carboxyl C_{60} in a yield of 62%. ^{13}C NMR (100 MHz, acetonitrile-d_3): δ 167.88, 141.44, 141.30, 69.36, 46.37.

2.3.3. C_{60}(*N*-methylpiperazine)$_4$

Fullerene C_{60} was dissolved in 1,2-dichlorobenzene for 2 h at ambient temperature. A solution of 1-methylpiperazine in 1,2-dichlorobenzene was then added in one portion to the fullerene solution. The resulting mixture was stirred in air under irradiation from the top by 60 W incandescent light bulb. The course of the reaction was monitored by thin layer chromatography (TLC) and stopped when conversion of C_{60} was complete. The reaction was then diluted by toluene (1:7 by volume) and poured into large amount of n-hexane to precipitate the unreacted fullerene. The resulting solution was filtered and purified by repetitive chromatography to afford C_{60}(N-methylpiperazine)$_4$.

2.3.4. C_{60}(1,1-dimethylpiperazin-1-ium)$_4$ (piperazine C_{60})

Compound C_{60}(*N*-methylpiperazine)$_4$ and sodium bicarbonate (10 equiv) were dissolved in $CHCl_3$ and purged with nitrogen gas. Iodomethane (10 equiv) was then dropped into the reaction and the mixture was allowed to stir at 50 °C for 24 h. The solution was cooled and added excess acetone to remove sodium bicarbonate by precipitation. The mixture was filtered and the residue was purified by repetitive chromatography to afford the orange product piperazine C_{60} in a yield of 85%. ^{13}C NMR (100 MHz, $CDCl_3$): δ 149.90-142.00 (fullerenic sp_2 carbons), 55.99, 50.31, 46.17.

2.4. Fabrication of LIBs and LIB tests

The battery tests were performed with CR2025-type coin cells containing the C_{60} or C_{60} derivatives working electrode. The working electrodes were prepared by a slurry coating method with 60 wt% of sample, 30 wt% conductive acetylene black, and 10 wt% polyvinylidene fluoride (PVDF) binder dispersed in *N*-methyl-2-pyrrolidone (NMP). The mass of each C_{60} and C_{60} derivatives thin film electrode was precisely measured with a microbalance before coin cell assembly. Coin cells were assembled in an argon-filled glove box with a metallic lithium foil as the combined reference and counter electrodes. The moisture content and oxygen level in the glove box were maintained less than 1 ppm. The electrolyte was 1 M $LiPF_6$ in a 1:1 (v/v) mixture of EC/DMC with Celgard 2300 polypropylene as separator. The cells were galvanostatically charged and discharged at a constant current density of 0.1 C based on the weight of the pristine C_{60} or C_{60} derivative sample on a battery test system (Arbin 2000-BT) for galvanostatic discharge–charge cycling tests ranging from 0.02 to 3.0 V. Cyclic voltammetry measurements were carried out on an electrochemistry workstation (CHI 760E) over the potential range 0.02 – 3.0 V vs. Li/Li^+ at a scan rate of 0.1 mV s^{-1}.

2.5. Calculation of specific capacity of C_{60} and C_{60} derivatives

The specific capacity of C_{60} and C_{60} derivatives can be calculated by the following formula:

$$C_t(mA{\cdot}h{\cdot}g^{-1}) = \frac{n \times F(C{\cdot}mol^{-1})}{M_w(g{\cdot}mol^{-1})} = \frac{n \times 96485(C)}{M_w(g)} = \frac{n \times 96485(A{\cdot}s)}{M_w(g)} = \frac{n \times 96485 \times 1000/3600(mA{\cdot}h)}{M_w(g)} = \frac{26801 \times n}{M_w} mA{\cdot}h{\cdot}g^{-1})$$

in the formula, C_t, n, F and M_w represents the theoretical specific capacity, the transferred electron number in each structural unit, the Faraday constant and the molecular weight of the structural unit, respectively. The molecular weights of C_{60}, ester C_{60}, carboxyl C_{60}, and positive piperazine C_{60} are 720, 2094.84, 1332, 1176.48, respectively.

It was found that the number of lithium intercalated in one C_{60} could reach 12 by electrochemical studies [58]. Based on this, the calculated the capacity of C_{60} is 446 mAh g^{-1}. For ester C_{60}, 12 carbonyl group in ester C_{60} can bind 12 lithium ions and C_{60} can bind 12 lithium ions ($Li_{12}C_{60}$), so the calculated capacity of ester C_{60} is 307 mAh g^{-1}. For carboxyl C_{60} anode, 12 of carboxyl group may bind 12 lithium ions [64], and the C_{60} core could complex 12 lithium ions [58]. So the total number of lithium ion storage could be 24 for one carboxyl C_{60} and the corresponding calculated capacity of lithium storage is 483 mAh g^{-1}.

3. Results and discussion

3.1. Synthesis and structural characterization of functionalized C_{60}s

Ester C_{60} and carboxyl C_{60}, were synthesized by following the literature procedures [61,62]. Briefly, ester C_{60} was made by treating deoxygenated C_{60} solution with sodium naphthalenide and excess amount of di-*tert*-butyl 2-bromo-2-methylmalonate. Carboxyl C_{60} was prepared by the hydrolysis of $C_{60}[C(CO_2Et)_2]_6$, which was made by the treatment of C_{60} with 9,10-dimethylanthracene, CBr_4, diethyl

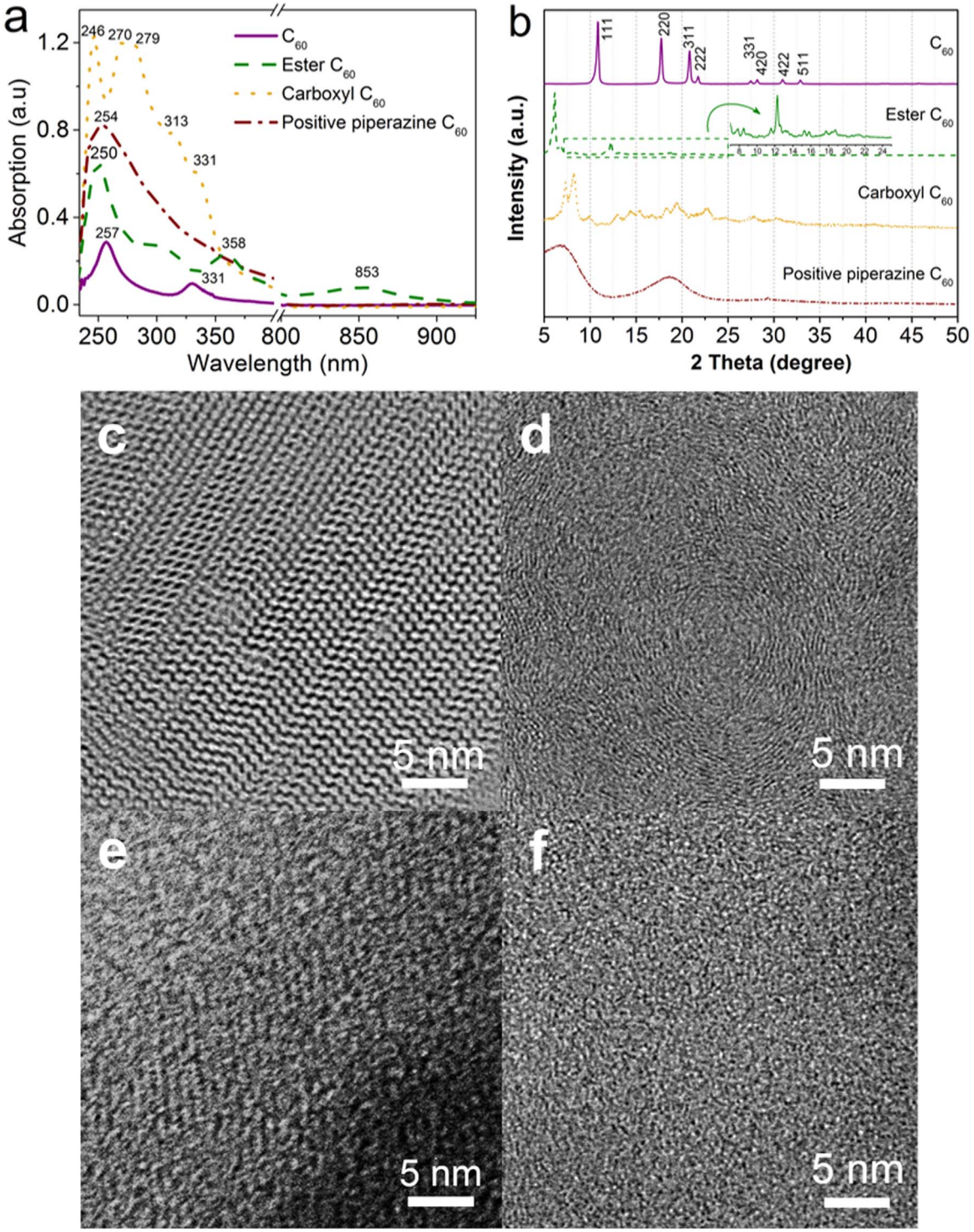

Fig. 2. (a) UV-visible spectra of four different C_{60}s in tetrahydrofuran solution including C_{60} (purple, solid), ester C_{60} (oliver, dash), carboxyl C_{60} (yellow, dot) and positive piperazine C_{60} (wine, dash dot); (b) XRD of C_{60} (purple, solid), ester C_{60} (oliver, dash), carboxyl C_{60} (yellow, dot) and positive piperazine C_{60} (wine, dash dot); (c-f) TEM images of C_{60} (c), ester C_{60} (d), carboxyl C_{60} (e), and positive piperazine C_{60} (f).

malonate, and excess amount of 1,8-diazabicyclo-[5.4.0]undec-7-ene. Piperazine C_{60} was synthesized by reacting C_{60}(*N*-methylpiperazine)$_4$ with iodomethane, in which C_{60}(N-methylpiperazine)$_4$ was prepared by treating C_{60} with 1-methylpiperazine in 1,2-dichlorobenzene [63]. The molecular structures of these three C_{60} derivative were confirmed by ^{13}C NMR spectroscopy (Fig. S1 – S3 in Supporting information).

The structures of four C_{60} and C_{60} derivatives are shown in Fig. 1b. Pristine C_{60} is molecule, without any functional group. Carboxyl C_{60} and ester C_{60} has 12 carboxyl and ester groups, respectively. Piperazine C_{60} has four positively-charged sites (ammonium salt) distributed on the northern hemisphere of the C_{60} (Fig. 1b) and hence is the only one with an asymmetric structure. Functionalization of C_{60} leads to modification of electronic structures and the optical images of the fullerene solutions reveal distinct colors (Fig. 1b), consistent with their corresponding UV–visible absorption spectra (see Fig. 2a) that will be elaborated later.

In Fig. 2a, pristine C_{60} has two prominent absorption peaks at 257 nm and 331 nm, which are typical for π - π* transitions in aromatic

systems [65]. Ester C_{60} has three obvious peaks at 250 nm, 358 nm and 853 nm. The 853 nm peak arises from the fully conjugated equatorial tranulene structure [61,66]. Carboxyl C_{60} has two shoulder bands around 331 nm and 313 nm, and strong absorption bands at 246 nm, 270 nm, and 279 nm [62]. The above spectra are in good agreement with those reported in previous literatures. As for piperazine C_{60}, it only shows one main absorption peak at 254 nm, presumably due to a highly asymmetric structure that disrupts the conjugation in the molecule.

The XRD was used for characterizing the crystalline structure of four different C_{60}s (Fig. 2b). Pristine C_{60} shows very strong (111), (220), and (311) peaks associated with single crystalline C_{60}, consistent with the results reported previously [67]. In contrast, ester C_{60} and carboxyl C_{60} show significantly reduced crystalline structure, as manifested by the much weaker diffraction patterns as compared to pristine C_{60}. Notably, ester C_{60} and carboxyl C_{60} have relatively sharp peaks in smaller angles of 6.1° and 7.0°, respectively, due to increased inter-C_{60} separation by the functional groups. The disruption of crystalline structure is particularly prominent in the case of piperazine C_{60} due to its structural asymmetry, which inhibits crystalline packing at various length scales. As a result, the XRD of piperazine C_{60} reveals an amorphous structure with only two broad peaks centered around 7° and 18° (Fig. 2b).

The TEM images are consistent with XRD results. In Fig. 2c, the TEM image of pristine C_{60} shows a perfect crystalline pattern with about 1.0 nm center-to-center distance between the molecules, consistent with the previous study [68]. The TEM image of ester C_{60} (Fig. 2d) and carboxyl C_{60} (Fig. 2e) only show some streaking patterns, which are consistent with the much weaker peaks in their corresponding XRD spectra. Piperazine C_{60} shows no structural order in its TEM image (Fig. 2f), again consistent with the two broad peaks in its XRD spectrum.

Electrochemical cyclic voltammograms (CVs) and specific surface area measurements on C_{60} and its derivatives (Fig. S4 and Table S1 in Supporting information) also revealed changes dominated by the nature and the regiochemistry of the functional groups. Such molecular-level-tunable structural, electronic and electrochemical properties in these C_{60} and C_{60} derivatives are expected to significantly impact their performances in LIBs, as will be examined below.

3.2. Lithium ion storage performance of functionalized C_{60}s

The C_{60}s were used as anode materials and assembled into a coin cell with lithium metal as counter and reference electrodes (see Materials and methods for details). Fig. 3 shows the discharge-charge curves (at current density of 0.1 C) and CVs of four different C_{60}-based LIBs for the initial three cycles. During discharging (intercalation of lithium ions) of pristine C_{60}, the voltage drops reveal several plateaus at 2.0–2.2 V, 1.7–1.9 V, and 1.5–1.7 V in Fig. 3a. The discharge and charge capacities in the first cycle are 653 and 163 mAh g^{-1}, respectively. The CV curve of pristine C_{60} (Fig. 3b) has three main peaks at 2.05 V, 1.78 V and 1.54 V that matches well with the charge/discharge voltage profiles in Fig. 3a. Ester C_{60} also shows the first discharging curve with several plateaus at 2.3–2.5 V, 2.1–2.3 V, 1.8–2.0 V, 1.5–1.7 V, 0.7–1.2 V (Fig. 3c) that again correspond well with its CV in Fig. 3d. The initial discharge and charge capacities of ester C_{60} are 680 mAh g^{-1} and 401 mAh g^{-1}, respectively, which are larger than those of pristine C_{60} presumably due to the ester groups on C_{60}. Yet more prominent improvements were observed for carboxyl C_{60} (Fig. 3e). The discharge and charge capacities of carboxyl C_{60} for the first cycle are 1373 and 773 mAh g^{-1}, respectively, which are much higher than those of pristine C_{60} and ester C_{60}. Interestingly, unlike the capacity improvements achieved for carboxyl and ester C_{60}s, we observed a relatively low discharge capacity of 335 mAh g^{-1} and charge capacity of 107 mAh g^{-1} in the first cycle for piperazine C_{60} (Fig. 3g), reflecting the counterproductive effect of positively-charged piperazine groups on the capacity performance of C_{60} in LIBs.

Notably, all these C_{60} and C_{60} derivatives show large irreversible capacities in the first cycle. For example, the carboxyl C_{60} has an irreversible capacity loss as high as 600 mAh g^{-1}, which is most likely due to the formation of solid electrolyte interphase (SEI) layer [5]. This process corresponds to the voltage plateau at 0.5–0.8 V consistent with the prominent peak in the battery CV (Fig. 3f). The formation of SEI layer is a common issue for most anode materials in LIBs and remains a challenge to be addressed in the future. Nonetheless, the discharging-charging cycles of all the C_{60}s eventually become stable after the 50th cycle (Figs. 3 and 4).

The cycling performances of four C_{60}s were evaluated at 0.1 C in the voltage range of 0.02–3 V (Fig. 4a). All the C_{60}s exhibit stable and reversible cycling behavior after the first few cycles, as manifested by their negligible capacity losses over 100 charging-discharging cycles. Pristine C_{60} shows a stabilized charging-discharging capacity of 170 mAh g^{-1} at the 100th cycle. Consistent with the observations in Fig. 3, the discharge capacity of piperazine C_{60} (83 mAh g^{-1} at the 100th cycle, Fig. 4a) is significantly lower than pristine C_{60} at all cycle stages. In comparison, carboxyl and ester C_{60}s exhibit a much higher capacity. Specifically, the discharge capacity of carboxyl C_{60} (ester C_{60}) is 1373 mAh g^{-1} (680 mAh g^{-1}) in the first cycle, 740 mAh g^{-1} (336 mAh g^{-1}) in the third cycle, and then gradually increases to and stabilizes at 861 mAh g^{-1} (404 mAh g^{-1}) after 100 cycles. The increase in capacities after the third cycle is attributed to the activating process of the anode [7]. To the best of our knowledge, these exceptionally high lithium ion storage capacities based on fullerenes materials have never been reported before. In particular, the capacity of carboxyl C_{60} is five time higher than pristine C_{60}, more than double the capacity of graphite (theoretical capacity of 372 mAh g^{-1}) [14], and higher than graphene (theoretical capacity of 744 mAh g^{-1}) [69]. In Fig. 4a, we also plot the coulombic efficiency of carboxyl C_{60}, which is 56.3% (at 0.1 C) for the first cycle and increases to 92.7% at the third cycle and above 99% after 7 cycles.

In addition to the high capacity and excellent cycling performance, we also studied the cycling stability of carboxyl C_{60} at very high charging/discharging rates (Fig. 4b). The cell was first discharged/charged at a current density of 0.1 C for 10 cycles, and then at various current densities from 0.5 to 5 C each for 10 cycles. The discharge capacities are 759, 638, 555, and 461 mAh g^{-1} at 0.1, 0.5, 1, and 2 C, respectively. Even at very high rate of 5 C (12 min to full charge), the discharge capacity is still as high as 378 mAh g^{-1}. After cycling at different rates and then returning to 0.1 C, the specific capacity is fully recovered to 773 mAh g^{-1}, showing a very stable cycling performance. In addition, the faster charge and discharge tests with long cycling (1 C for 300 cycles) were carried out and the results are shown in Fig. 4c. Notably, the carboxyl-C_{60}-electrode capacity of ca. 560 mAh g^{-1} was retained after 300 cycles, which corresponds to a 97.7% capacity retention at the rate of 1 C, indicating its extremely stable cycling performance.

3.3. Mechanisms for the structure-property-performance correlation

Here we propose the mechanisms responsible for the observed dependence of C_{60} LIB performances on functional groups (Fig. 5). It was reported, through electrochemical studies, that the number of lithium intercalated in one C_{60} molecule could reach 12, i.e., on average 5 carbon atoms per lithium (LiC_5); this number is higher than graphite (LiC_6) [58]. Based on this number, the calculated capacity of C_{60} can be as high as 446 mAh g^{-1} (see calculation method in Supporting information). This value is, however, much higher than the experimental value of 170 mAh g^{-1} for pristine C_{60} (Figs. 3 and 4). The large discrepancy likely results from the highly crystalline nature of C_{60} with densely pack structure and small specific surface area (1.69 m^2 g^{-1}, Table S1 in Supporting information), which limits the diffusion and reversible intercalation of lithium ions in C_{60}.

By functionalizing C_{60} with 12 ester groups or 12 carboxyl groups, the reversible capacity of ester C_{60} and carboxyl C_{60} can reach

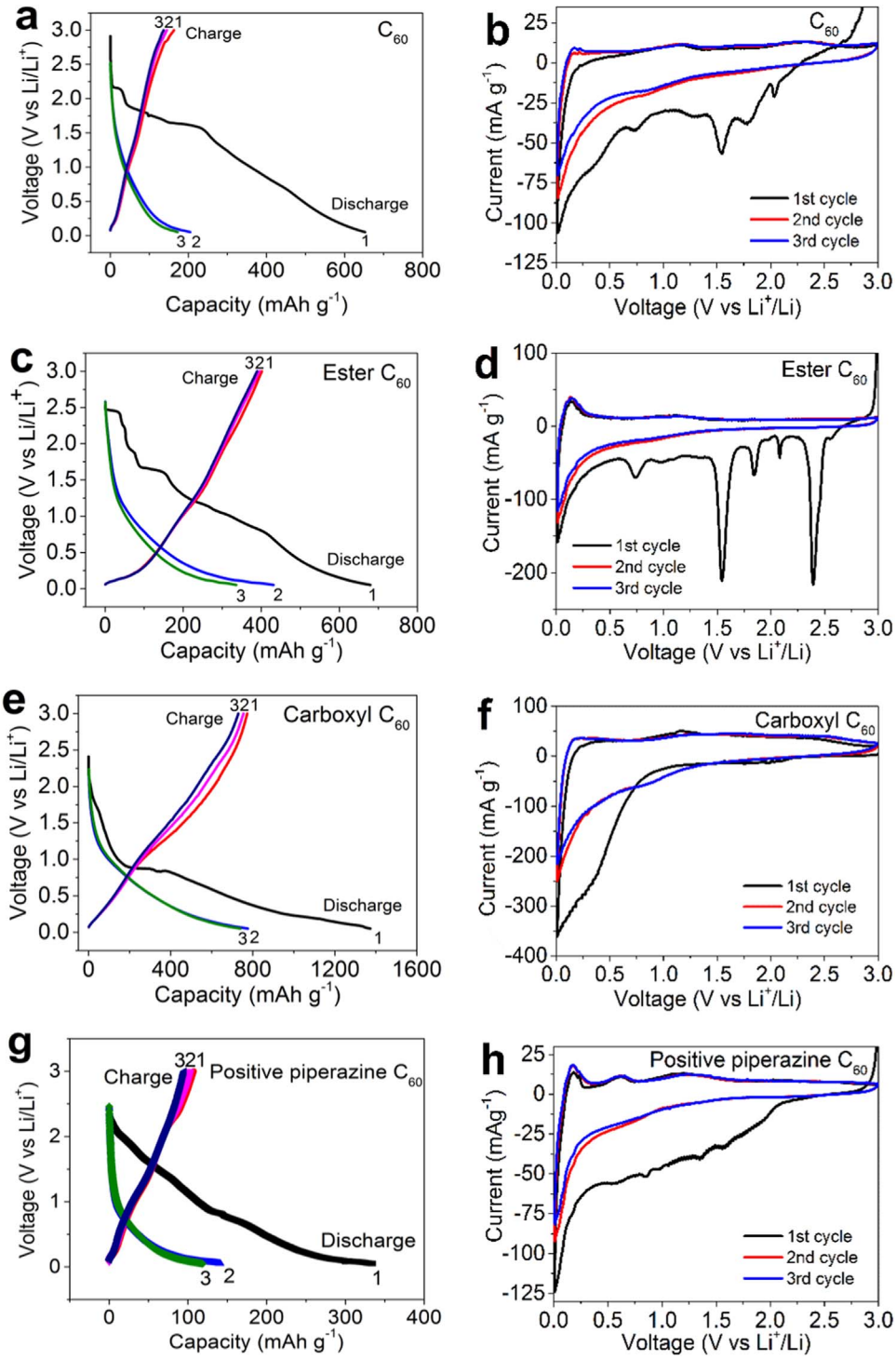

Fig. 3. (a), (c), (e), and (g) are discharge-charge profiles at a rate of 0.1 C for the initial three cycles of C_{60}, ester C_{60}, carboxyl C_{60}, and piperazine C_{60}, respectively. (b), (d), (f), and (h) are cyclic voltammograms at a scan rate of 0.1 mV s^{-1} for the initial three cycles of studied C_{60} anodes.

404 mAh g^{-1} and 861 mAh g^{-1}, respectively. It was suggested that the incorporation of carboxylate and/or ester functional groups in anode materials can improve the LIB capacity due to a high binding energy between O=C-O functional groups and lithium ions [27,64]. Taking this factor into consideration and adding up the lithium storage capacities of C_{60} and carbonyl groups [58], the calculated capacities of ester C_{60} and carboxyl C_{60} are ~ 307 mAh g^{-1} and 483 mAh g^{-1}, respectively. Both are lower than the corresponding experimental values. The higher capacity observed can be rationalized as below. Our recent experimental and theoretical studies on nanographene materials demonstrated that the charge capacity of nanographenes can be increased/decreased by functionalizing the nanographene with electron donating/withdrawing groups, respectively [50]. Electron donating groups increase the electron density on nanographene flakes allowing stabilizing greater number of positively charged lithium ions. Thus, the electron-donating nature of ester groups and carboxylate groups have significantly increased the electron density of the C_{60} thus allowing complex with greater number of lithium ions, *i.e.*, promoting the intercalation of more lithium ions into the more electron-rich C_{60} cage. Yet another factor, which contribute to the capacity increase, is the microstructural changes induced by the functional groups, including the less-crystalline structure (larger lattice void space, see Fig. 2) and larger specific surface area (Table S1) of ester and carboxyl C_{60}s than pristine C_{60}. To summarize, the ester and carboxylate groups can bind lithium ions,

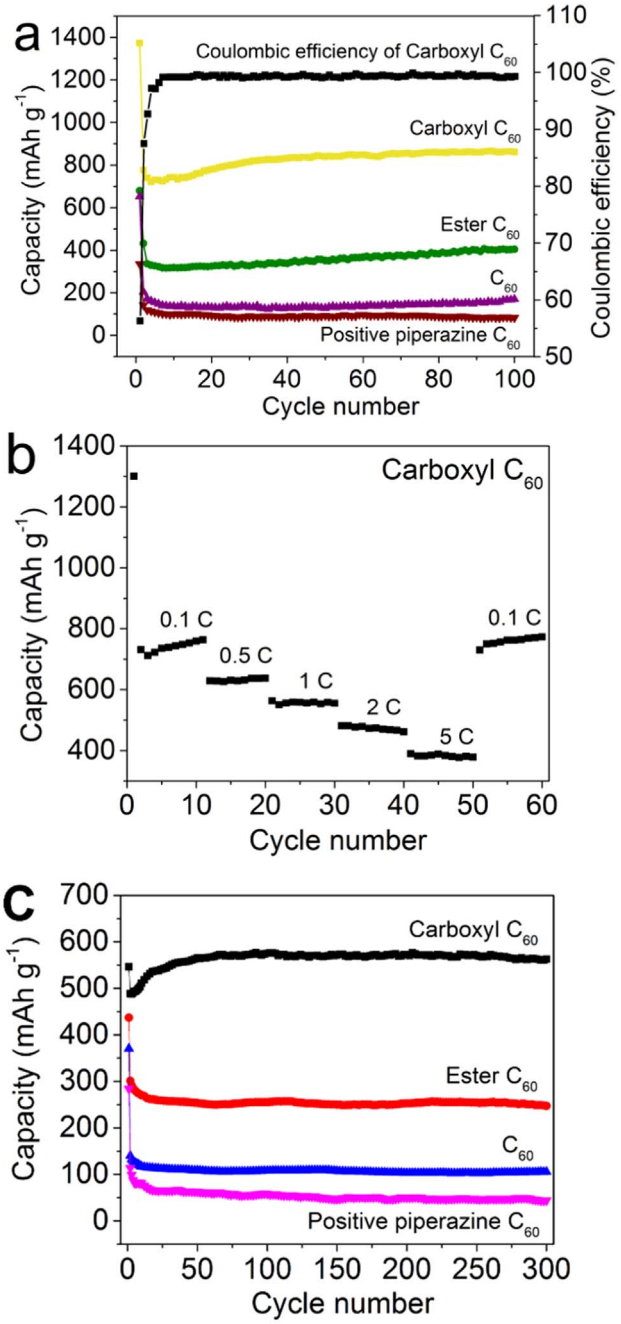

Fig. 4. (a) Cycling discharge-charge performance of pristine C_{60} and C_{60} derivatives for LIBs and coulombic efficiency of carboxyl C_{60} at 0.1 C; (b) rate performance of carboxyl C_{60}; (c) cycling stability of C_{60} and C_{60} derivatives for LIBs at a rate of 1 C.

donate electrons to the C_{60} cage, and increase the lattice void space and specific surface area for lithium intercalation, all of which result in the high capacity of ester C_{60} in LIBs.

Although the ester and carboxylate groups behave similarly in terms of inducing electronic and microstructural changes, the experimental capacity of carboxyl C_{60} (861 mAh g^{-1}) is significantly higher than that of ester C_{60} (404 mAh g^{-1}), the reason can be attributed to the neutral vs negatively-charged nature of ester and carboxylate groups, respectively. Very important to note that, the carboxylate C_{60} layer has an overall negative charge which can facilitate the insertion of positively-charged lithium ions through electrostatic attraction. This result is also consistent with the lower capacity of piperazine C_{60}. Indeed, the low capacity of 83 mAh g^{-1} observed for piperazine C_{60} is resulting from the electrostatic repulsion force between the positively charged piperazine groups and lithium ions. We note that the electron-withdrawing nature of piperazine groups might be another reason for the low capacity. This comparison suggests that C_{60}s functionalized with carboxyl/carboxylate groups are promising materials for LIB anodes. In summary, our studies provide a proof-of-principle demonstration that the performance of LIB can be optimized through tailored synthesis of C_{60} with functional group and hierarchical structure that can lead to establishment of structure-property correlation previously not accessible.

4. Conclusion

In summary, we have demonstrated, for the first time, C_{60} and its derivatives with well-defined molecular structures as anode materials in LIBs. Four different C_{60}s including pristine, ester, carboxyl, and piperazine C_{60}, were thoroughly characterized by NMR, TEM, UV–visible spectroscopy, and XRD in terms of their structure and morphology. Then the relationship between the molecular structures and lithium ion storage properties was established to provide guidance to rational design of organic compound-based electrodes for LIBs. The carboxyl C_{60} based LIBs showed the highest charge capacity of 861 mAh g^{-1} after 100 charging-discharging cycles with nearly 100% columbic efficiency. This is significantly higher than those of pristine C_{60} (170 mAh g^{-1}), ester C_{60} (404 mAh g^{-1}), and piperazine C_{60} (83 mAh g^{-1}), and is also superior than commercial graphite (theoretical capacity of 372 mAh g^{-1}) and graphene (theoretical capacity of 744 mAh g^{-1}). We discovered that C_{60} derivatives can be a highly efficient LIB anode material. The results strongly suggest that superior exceptional performance of carboxyl C_{60} links to a combination of several structural parameters. They include a complex formation between lithium ions and oxygen atoms on the carboxyl group *i.e.,* strong Li binding sites provided by O=C-O. The improved lithium-binding capability of C_{60} cage is also due to increased electron density resulting from electron donating nature of carboxylate groups. Furthermore, the electrostatic attraction between carboxylate groups and lithium ions, the large lattice void space, and high specific area have all contributed to the excellent LIB properties. Most importantly, the structure-property-performance relationship established in this work suggests that C_{60} derivatives are very promising anode materials through a functionalization with desired substituents. Accurate controls of molecular structure, surface charge, crystalline packing, specific surface area, and electrochemical property impact the performance of lithium-ion storage. This work offers new insights and directions that tailoring synthesis of C_{60} derivatives or any other organic compounds with optimal functional groups can lead to new types of highly efficient carbon-based materials for energy storage.

Acknowledgment

The authors would like to acknowledge financial support by the Laboratory Directed Research and Development (LDRD) program (G. Wu, and H.-L. Wang) at Los Alamos National Laboratory (LANL). H.-L. Wang also acknowledges the start-up fund from Southern University of Science and Technology, China. C. Shan thanks the Director's Fellowship at Los Alamos National Laboratory for supporting the synthesis of carbon materials and lithium-ion batteries fabrication. G. Wu also acknowledges the start-up fund from the University at Buffalo (SUNY) along with the National Science Foundation (CBET-1511528).

Appendix A. Supporting information

Supplementary data associated with this article can be found in the online version at http://dx.doi.org/10.1016/j.nanoen.2017.08.033.

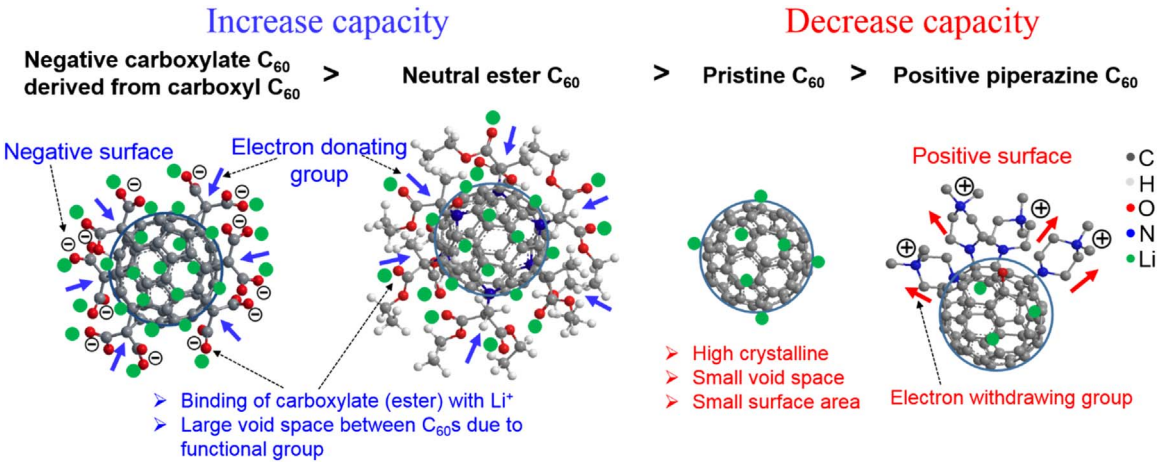

Fig. 5. Schematic mechanism for elucidating the relationship between functionalization and capacity of C_{60} and its derivatives in LIBs.

References

[1] K.-X. Wang, X.-H. Li, J.-S. Chen, Adv. Mater. 27 (2015) 527–545.
[2] P.G. Bruce, B. Scrosati, J.-M. Tarascon, Angew. Chem. Int. Ed. 47 (2008) 2930–2946.
[3] C.K. Chan, H. Peng, G. Liu, K. McIlwrath, X.F. Zhang, R.A. Huggins, Y. Cui, Nat. Nanotechnol. 3 (2008) 31–35.
[4] F. Cheng, J. Liang, Z. Tao, J. Chen, Adv. Mater. 23 (2011) 1695–1715.
[5] Z. Sun, L. Zhang, F. Dang, Y. Liu, Z. Fei, Q. Shao, H. Lin, J. Guo, L. Xiang, N. Yerra, Z. Guo, CrystEngComm 19 (2017) 3288–3298.
[6] L. Zhang, W. Yu, C. Han, J. Guo, Q. Zhang, H. Xie, Q. Shao, Z. Sun, Z. Guo, J. Electrochem. Soc. 164 (2017) H651–H656.
[7] L. Qie, W.M. Chen, Z.H. Wang, Q.G. Shao, X. Li, L.X. Yuan, X.L. Hu, W.X. Zhang, Y.H. Huang, Adv. Mater. 24 (2012) 2047–2050.
[8] A. Rosenman, E. Markevich, G. Salitra, D. Aurbach, A. Garsuch, F.F. Chesneau, Adv. Energy Mater. 5 (2015) 1500212.
[9] J.C. Bachman, S. Muy, A. Grimaud, H.-H. Chang, N. Pour, S.F. Lux, O. Paschos, F. Maglia, S. Lupart, P. Lamp, L. Giordano, Y. Shao-Horn, Chem. Rev. 116 (2016) 140–162.
[10] Y. Tang, Y. Zhang, W. Li, B. Ma, X. Chen, Chem. Soc. Rev. 44 (2015) 5926–5940.
[11] X. Wang, Q. Weng, Y. Yang, Y. Bando, D. Gotberg, Chem. Soc. Rev. 45 (2016) 4042–4073.
[12] G. Chen, L. Yan, H. Luo, S. Guo, Adv. Mater. 28 (2016) 7580–7602.
[13] X. Gu, F. Wu, B. Lei, J. Wang, Z. Chen, K. Xie, Y. Song, D. Sun, L. Sun, H. Zhou, F. Fang, J. Power Sources 320 (2016) 231–238.
[14] J.M. Tarascon, M. Armand, Nature 414 (2001) 359–367.
[15] Y.P. Wu, E. Rahm, R. Holze, J. Power Sources 114 (2003) 228–236.
[16] L.-Z. Bai, D.-L. Zhao, T.-M. Zhang, W.-G. Xie, J.-M. Zhang, Z.-M. Shen, Electrochim. Acta 107 (2013) 555–561.
[17] N. Mahmood, T.Y. Tang, Y.L. Hou, Adv. Energy Mater. 6 (2016) 1600374.
[18] Z.H. Xiang, Q.B. Dai, J.F. Chen, L.M. Dai, Adv. Mater. 28 (2016) 6253–6261.
[19] R. Liu, D. Li, C. Wang, N. Li, Q. Li, X. Lü, J.S. Spendelow, G. Wu, Nano Energy 6 (2014) 73.
[20] C. Wang, D. Higgins, F. Wang, D. Li, R. Liu, G. Xia, N. Li, Q. Li, H. Xu, G. Wu, Nano Energy 9 (2014) 334.
[21] A. Casimir, H. Zhang, O. Ogoke, J.C. Amine, J. Lu, G. Wu, Nano Energy 27 (2016) 359.
[22] G. Tan, F. Wu, Y. Yuan, R. Chen, T. Zhao, Y. Yao, J. Qian, J. Liu, Y. Ye, R. Shahbazian-Yassar, J. Lu, K. Amine, Nat. Commun. 7 (2016) 11774.
[23] Y. Zhao, X. Li, B. Yan, D. Xiong, D. Li, S. Lawes, X. Sun, Adv. Energy Mater. 6 (2016).
[24] X. Han, G. Qing, J. Sun, T. Sun, Angew. Chem. Int. Ed. 51 (2012) 5147–5151.
[25] Z. Song, H. Zhou, Energy Environ. Sci. 6 (2013) 2280–2301.
[26] B. Haeupler, A. Wild, U.S. Schubert, Adv. Energy Mater. 5 (2015) 1402034.
[27] J. Xie, Q. Zhang, J. Mater. Chem. A4 (2016) 7091–7106.
[28] J. Liu, T. Zhao, S. Zhang, Q. Wang, Nano Energy 38 (2017) 263–270.
[29] A.L.M. Reddy, A. Srivastava, S.R. Gowda, H. Gullapalli, M. Dubey, P.M. Ajayan, ACS Nano 4 (2010) 6337–6342.
[30] J.-G. Wang, K. Xie, B. Wei, Nano Energy 15 (2015) 413–444.
[31] L. Dai, D.W. Chang, J.-B. Baek, W. Lu, Small 8 (2012) 1130–1166.
[32] G. Wang, X. Shen, J. Yao, J. Park, Carbon 47 (2009) 2049–2053.
[33] W. Sun, Y. Wang, Nanoscale 6 (2014) 11528–11552.
[34] Z.-S. Wu, W. Ren, L. Xu, F. Li, H.-M. Cheng, ACS Nano 5 (2011) 5463–5471.
[35] Y. Liu, X. Wang, Y. Dong, Z. Wang, Z. Zhao, J. Qiu, J. Mater. Chem. A 2 (2014) 16832–16835.
[36] B.J. Landi, M.J. Ganter, C.D. Cress, R.A. DiLeo, R.P. Raffaelle, Energy Environ. Sci. 2 (2009) 638–654.
[37] C. Kang, M. Patel, B. Rangasamy, K.-N. Jung, C. Xia, S. Shi, W. Choi, J. Power Sources 299 (2015) 465–471.
[38] A. Zhang, X. Fang, C. Shen, Y. Liu, C. Zhou, Nano Res. 9 (2016) 3428–3436.
[39] J.-C. Chang, Y.-F. Tzeng, J.-M. Chen, H.-T. Chiu, C.-Y. Lee, Electrochim. Acta 54 (2009) 7066–7070.
[40] K. Tang, R.J. White, X. Mu, M.-M. Titirici, P.A. van Aken, J. Maier, ChemSusChem 5 (2012) 400–403.
[41] J. Yi, X.P. Li, S.J. Hu, W.S. Li, L. Zhou, M.Q. Xu, J.F. Lei, L.S. Hao, J. Power Sources 196 (2011) 6670–6675.
[42] J. Yang, X.-y. Zhou, Y.-l. Zou, J.-j. Tang, Electrochim. Acta 56 (2011) 8576–8581.
[43] K.T. Lee, J.C. Lytle, N.S. Ergang, S.M. Oh, A. Stein, Adv. Funct. Mater. 15 (2005) 547–556.
[44] R.R. Gaddam, D. Yang, R. Narayan, K.V.S.N. Raju, N.A. Kumar, X.S. Zhao, Nano Energy 26 (2016) 346–352.
[45] M.-S. Balogun, W. Qiu, F. Lyu, Y. Luo, H. Meng, J. Li, W. Mai, L. Mai, Y. Tong, Nano Energy 26 (2016) 446–455.
[46] J. Zhang, Y.-S. Hu, J.-P. Tessonnier, G. Weinberg, J. Maier, R. Schloegl, D.S. Su, Adv. Mater. 20 (2008) 1450–1455.
[47] L. Wen, F. Li, H.-M. Cheng, Adv. Mater. 28 (2016) 4306–4337.
[48] E. Yoo, J. Kim, E. Hosono, H.-s. Zhou, T. Kudo, I. Honma, Nano Lett. 8 (2008) 2277–2282.
[49] H.R. Byon, B.M. Gallant, S.W. Lee, Y. Shao-Horn, Adv. Funct. Mater. 23 (2013) 1037–1045.
[50] H.-J. Yen, H. Tsai, M. Zhou, E.F. Holby, S. Choudhury, A. Chen, L. Adamska, S. Tretiak, T. Sanchez, S. Iyer, H. Zhang, L. Zhu, H. Lin, L. Dai, G. Wu, H.-L. Wang, Adv. Mater. 28 (2016) 10250–10256.
[51] H.W. Kroto, J.R. Heath, S.C. Obrien, R.F. Curl, R.E. Smalley, Nature 318 (1985) 162–163.
[52] S. Schein, T. Friedrich, Proc. Natl. Acad. Sci. USA 105 (2008) 19142–19147.
[53] Z. Chen, L. Ma, Y. Liu, C. Chen, Theranostics 2 (2012) 238–250.
[54] R. Partha, J.L. Conyers, Int. J. Nanomed. 4 (2009) 261–275.
[55] M. Gruber, J. Wagner, K. Klein, U. Hoermann, A. Opitz, M. Stutzmann, W. Bruetting, Adv. Energy Mater. 2 (2012) 1100–1108.
[56] R. Charvet, Y. Yamamoto, T. Sasaki, J. Kim, K. Kato, M. Takata, A. Saeki, S. Seki, T. Aida, J. Am. Chem. Soc. 134 (2012) 2524–2527.
[57] J.L. Segura, N. Martin, D.M. Guldi, Chem. Soc. Rev. 34 (2005) 31–47.
[58] Y. Chabre, D. Djurado, M. Armand, W.R. Romanow, N. Coustel, J.P. McCauley, J.E. Fischer, A.B. Smith, J. Am. Chem. Soc. 114 (1992) 764–766.
[59] R.O. Loutfy, S. Katagiri, Springer Netherlands, pp. 357–367, 2002.
[60] J. Minwoong, H. Young-Kyu, L. Kwang-Ryeol, H. Mizuseki, K. Seungchul, Carbon 77 (2014) 1140–1147.
[61] T. Canteenwala, P.A. Padmawar, L.Y. Chiang, J. Am. Chem. Soc. 127 (2005) 26–27.
[62] M. Rebecca, W. Hsing-Lin, G. Jun, I. Srinivas, M.A. Gabriel, M. Jennifer, S.P. Andrew, Y.P. Bao, W. Chun-Chih, C. Zhong, G. Yuan, I. Rashi, Toxicol. Appl. Pharmacol. 234 (2009) 58–67.
[63] O.A. Troshina, P.A. Troshin, A.S. Peregudov, V.I. Kozlovski, R.N. Lyubovskaya, Chem. Eur. J. 12 (2006) 5569–5577.
[64] S. Renault, D. Brandell, T. Gustafsson, K. Edstrom, Chem. Commun. 49 (2013) 1945–1947.
[65] I.P. Romanova, A.V. Bogdanov, I.A. Izdelieva, V.A. Trukhanov, G.R. Shaikhutdinova, D.G. Yakhvarov, S.K. Latypov, V.F. Mironov, V.A. Dyakov, I.V. Golovnin, D.Y. Paraschuk, O.G. Sinyashin, Beilstein J. Org. Chem. 10 (2014) 1121–1128.
[66] X.W. Wei, A.D. Darwish, O.V. Boltalina, P.B. Hitchcock, J.M. Street, R. Taylor, Angew. Chem. Int. Ed. 40 (2001) 2989–2992.
[67] B.M. Ginzburg, S. Tuichiev, S.K. Tabarov, A.A. Shepelevskii, L.A. Shibaev, Tech. Phys. 50 (2005) 1458–1461.
[68] A. Goel, J.B. Howard, J.B. Vander Sande, Carbon 42 (2004) 1907–1915.
[69] G.X. Wang, X.P. Shen, J. Yao, J. Park, Carbon 47 (2009) 2049–2053.

Changsheng Shan is a postdoctoral fellow at Los Alamos National Laboratory (LANL). He obtained his B.S. at Northeast Normal University at 2005 and Ph.D. at Changchun Institute of Applied Chemistry in 2011 followed by extensive postdoctoral trainings at City University of Hong Kong (2011–2012), University of Delaware (2012–2014), and Indiana University (2014–2016). He was trained in materials electrochemistry from his graduate education and his current research focuses on developing functional nanomaterials for electrochemical applications in energy storage and analysis.

Hungju Yen completed his Ph.D. degree with the *1st prize of PhD graduates* from National Taiwan University in 2011. He joined Los Alamos National Laboratory as the *J. Robert Oppenheimer Distinguished Postdoctoral Fellow*. Dr. Yen's main research interest lies in the organic synthesis of electroactive polymers and functional nanographenes with tailored optical and electronic properties. He has published more than 65 peer-reviewed papers in highly impact and influential journals. He also has 6 invited review article, 3 book chapter, 8 patents, and 100 conference papers. Now, he has more than 2200 citations for his papers with *h*-Index of 29.

Kaifeng Wu received his BS degree in Materials Physics from University of Science and Technology of China in 2010 and his PhD degree in Chemistry from Emory University in 2015. He is now a Professor in the State Key Laboratory of Molecular Reaction Dynamics at Dalian Institute of Chemical Physics, Chinese Academy of Sciences. His research interest is ultrafast spectroscopy and dynamics in energy related materials.

Qianglu Lin received his BS in Applied Chemistry from Shantou University in 2009, China; M.S. and Ph.D. in Chemical Engineering from New Mexico State University in 2010 and 2014, respectively. Qianglu conducted his Ph.D. thesis in the quantum dots group at Los Alamos National Laboratory and he then became a Postdoctoral Fellow in the same group. Qianglu's research activities focus on the synthesis, optical properties and device applications of core-shell quantum dots. He has authored 23 peer-reviewed journal publications in Nature Communications, ACS Nano, Nano Letters, Journal of American Chemical Societies, etc.

Ming Zhou received Ph.D degree from Changchun Institute of Applied Chemistry, sChinese Academy of Sciences in 2011. During 2011–2015, he did postdoctoral work at University of California, San Diego, Case Western Reserve University, University of Washington and Los Alamos National Laboratory (as a prestigious Director's Postdoctoral Fellow), respectively. Then, he joined Department of Chemistry at Northeast Normal University as a Full Professor through the successful selection of Recruitment Program of Global Youth Experts launched by Chinese government. He has published more than 50 papers with over 3700 citations (H-index: 29). His research interests include nanomaterials for analysis and energy applications.

Xiaofeng Guo is an assistant professor of the Department of Chemistry and the Alexandra Navrotsky Institute for Experimental Thermodynamics at Washington State University. Dr. Guo got his Ph.D. in Chemistry from the University of California, Davis in 2014 and was a G. T. Seaborg Postdoctoral fellow at Los Alamos National Laboratory (2015–2017). His current research interests are thermodynamics of actinides (transuranium)-containing phases, nuclear fuels and wastes; nanosized composites in the nuclear application; actinide-containing minerals crystallization and dissolution under hydrothermal conditions; and behaviors of materials under high temperature and high pressure. He has published 30 papers in the fields of material science, chemistry, geology, and thermodynamics.

Di Wu is an Assistant Professor in Chemical Engineering in the Voiland School of Chemical Engineering and Bioengineering at Washington State University, where he is also affiliated with Department of Chemistry and Materials Science & Engineering. His research focuses on thermodynamics of materials, catalysis, and surface chemistry related to energy and environmental sustainability. He earned his B.S. (2006) from Zhejiang University, China, M.S. (2008) from the University of Akron, and Ph.D. (2012) under the guidance of Alexandra Navrotsky from the University of California, Davis, all in Chemical Engineering. He also did postdoctoral research under Prof. Navrotsky from 2013 to 2016.

Hanguang Zhang is a Ph.D. student at University at Buffalo, SUNY. He obtained his Bachelor and Master degrees from Sichuan University (2013) and UB (2015), respectively. His research project is to synthesize three-dimensional porous carbon materials for energy conversion and storage.

Gang Wu is an Assistant Professor in the Department of Chemical and Biological Engineering at the University at Buffalo (SUNY-Buffalo). He completed his Ph.D. studies at the Harbin Institute of Technology in 2004 followed by extensive postdoctoral trainings at Tsinghua University (2004–2006), the University of South Carolina (2006–2008), and Los Alamos National Laboratory (LANL) (2008–2010). Then he was a staff scientist at LANL until he joined SUNY-Buffalo in 2014. His research focuses on functional materials and catalysts for electrochemical energy storage and conversion. He has written more than 150 papers with a citation of > 10,000 times.

Hsing-Lin Wang received his BS from Chemistry Department, National Chung Hsing University, Ph.D. in Chemistry from University of South Florida in 1992. He then became a Postdoctoral Fellow at University of Pennsylvania from 1993–1995. He came to Los Alamos National Laboratory as a Postdoctoral Fellow at 1995 and became a scientist in 1998. In 2016, he joined Southern University of Science and technology , Shenzhen China。 Hsing-Lin Wang's research activities mainly in organic synthesis, processing and applications of functional polymers, fullerenes derivatives, and nanostructured materials. He has authored 2 book chapters, 170 peer-reviewed publications and 20 issued patents and 4 patents pending. He is the editor of two specific issues in "Polymers" and "Journal of Nanomaterials.